

Article

Energy Analysis of a NZEB Office Building with Rooftop PV Installation: Exploitation of the Employees' Electric Vehicles Battery Storage

George Stamatellos , Olympia Zogou  and Anastassios Stamatelos * 

Department of Mechanical Engineering, University of Thessaly, 383 34 Volos, Greece

* Correspondence: stam@uth.gr; Tel.: +30-24210-74067

Abstract: Near zero energy buildings are increasing worldwide, exploiting low-carbon technologies in heating and electricity self-production. Commercial buildings are increasingly considered as candidates for the installation of smart micro-grids, which may profit from the added storage capacity of the batteries of employees electric vehicles, stationed during daytime in their charging lots. Smart exploitation of the interaction of these electricity sources and sinks may prove essential to address the complex electricity network demand patterns in today's fast changing energy mixture. The interaction of an efficient office building's energy system with a big rooftop photovoltaic installation and the aggregate storage capacity of 40 electric cars that are connected in the building's charging lots is studied by means of transient simulation in TRNSYS environment. The 18-zone building's heating, ventilation, and air conditioning system, the cars' batteries, and photovoltaic systems' interactions are analyzed on a monthly, seasonal, and hourly basis, against the respective demand curves of the Greek network. The results suggest that the specific system's size may profitably support the operation of a smart micro-grid. The total annual electricity consumption of the building is computed to reach 112,000 kWh, or 20 kWh/m²y. The annual electricity needs of the 40 electric cars, amounting to 101,000 kWh, can be fully met with 30% of the photovoltaic electricity production. Thus, the building becomes a net exporter of electricity to the network, with maximum exported electricity occurring daily between 12:00 and 14:00, which is favorable to meeting the demand curve. Thus, the establishment of smart micro-grids in commercial buildings with large rooftop photovoltaic panels' capacity and a significant number of electric cars in the employees' car fleet is quite effective in this direction.

Keywords: PV panels; battery storage; electric cars; ground-source heat pumps; building energy simulation; electricity load curve; smart grids



Citation: Stamatellos, G.; Zogou, O.; Stamatelos, A. Energy Analysis of a NZEB Office Building with Rooftop PV Installation: Exploitation of the Employees' Electric Vehicles Battery Storage. *Energies* **2022**, *15*, 6206. <https://doi.org/10.3390/en15176206>

Academic Editors: Jingyu Cao, Wei Wu, Mingke Hu and Yunfeng Wang

Received: 27 July 2022

Accepted: 23 August 2022

Published: 26 August 2022

Publisher's Note: MDPI stays neutral with regard to jurisdictional claims in published maps and institutional affiliations.



Copyright: © 2022 by the authors. Licensee MDPI, Basel, Switzerland. This article is an open access article distributed under the terms and conditions of the Creative Commons Attribution (CC BY) license (<https://creativecommons.org/licenses/by/4.0/>).

1. Introduction

The rapid increase of the share of electric vehicles (EV) in the international car fleet is pushed by the need of achieving net zero carbon emissions by 2050, with the electricity produced from low-carbon sources. The prevailing issue here is the EV charging, with recharging needed every 150–300 km. Battery charging requires a few hours with the car connected to the charger. Although quite significant investment has been carried out in charging infrastructure with about 2 million public charging points worldwide, this number should increase by two orders of magnitude in order to meet net zero emissions goals by 2050. For this reason, several countries are planning to require new buildings to be equipped with EV chargers [1]. Subsidizing EV sales must be combined with financial incentives to private companies for the operation of public chargers' networks. According to the prediction of several researchers, public chargers will be installed at an increasing rate during the next decade [2]. In the long run, the EV charging infrastructure is contemplated to combine powerful chargers that are installed on motorways, with low power chargers

available at houses or car parks of commercial buildings and shopping centers [3]. Grid-efficient charging is critical to the success of EVs integration to the grid. Legislation is being prepared to charge a higher price to EV drivers for unconditional charging their cars [4]. Thus, the integration of photovoltaic (PV) systems and electric vehicles (EVs) challenges the grid with increased peak loads and component overloading. A study predicted a 30% increase of the local peak load with a steeper evening ramp in a residential feeder circuit of 150 homes with 25% EV penetration [5]. Naturally, such effects would be relaxed by the introduction of delayed or smart charging along with the damping effect of the aggregation of households in large urban areas. Optimal matching between PV generation and EV load may further relax these adverse effects. Fachrizal et al. [6] optimized a PV-EV sizing framework for workplace PV powered chargers with load matching, introducing a new performance metric combining self-consumption (SC) and self-sufficiency (SS). Osório et al. [7] surveyed state-of-the-art concepts of PV panels, EVs, and batteries, to support the concept of rooftop PV powered parking lots. Bhatti et al. [8] reviewed some important aspects of PV-EV charging. Casella et al. [9] comparatively presented optimization models for the integration of EVs and charging stations (CSs). The focus was on the positioning and sizing of CSs and the optimal scheduling of EVs in smart grids, microgrids, and buildings, exploiting vehicle-grid (V2G) capabilities. Alkawsii et al. surveyed renewable energy charging infrastructure studies [10]. The integration of the rooftop PV installations with EV charging, significantly reduces the cost per km and the burden to the grid.

The on-going building heating electrification that is carried out by the increasing penetration of heat pumps, affects the electricity demand curves. Moreover, morning and evening ramp rates increase and require more flexible power plant capacity during winter months [11]. On the other hand, summer heat waves are becoming more frequent due to global warming, causing rapid demand increases during the day. For this reason, the added effect of EV charging in the electricity demand must be monitored. The smart management of electricity use can mitigate peaks in demand by shifting consumption to more favorable time slots. Further electrification of commercial buildings does not significantly affect the evening ramp, since they mainly require electricity during the daytime, which better matches the electricity production profile of the PV installations. Moreover, the application of advanced technologies as ground-coupled heat pumps in commercial buildings, results in the damping of oscillations during start-stop operation, which improves the demand patterns. Since the electricity consumption of EVs stays in the range of 0.1–0.2 kWh/km [12], the continuing improvements in building energy performance allow for increased EV charging. Nearly zero-energy buildings (NZEB) cover their low energy consumption mostly by renewable sources. In particular, the electrification of commercial buildings is favored by the shift to ground-source [13] or dual-source heat pumps [14], instead of the air-source heat pumps that are usually installed in single family houses. The increase in PV installations in commercial buildings enables the future operation of semiautonomous renewable energy sources' micro-grids [15]. In these cases, load profiling and forecasting is a necessary process that can be based on the exploitation of actual operation data by machine learning [16]. Machine learning tools additionally allow for the forecasting of the micro-grids PV self-production with increasing accuracy [17]. More generally, the upcoming highly renewable European electricity network gains significant advantages from cooperation among the connected smart grids [18]. In this context, Cebulla et al. [19] presented an analysis of the required storage capacity to support the increase of variable renewables in Europe. They optimized the required spatial distribution of storage along with the regionally prevailing renewable technologies and their temporal feed-in characteristics. A major challenge that must be addressed is the inherently limited dispatchability of renewable power generator sources. Now, it is essential that dispatchability be increased also at the micro-grid level, where PV panels are supported by battery units and other power sources. Whenever the main grid is overloaded, micro-grids support it with resilient power. This type of energy hub can run independently

and occasionally connected to the main grid. Thus, research is on-going with advanced micro-grid design, studying the complex trade-offs between risk tolerance and payback of capital investment. Several research works have investigated the integration of energy efficient buildings with rooftop PV installations in residential grids [20]. Experiments have been reported with rooftop PV systems with electric battery storage. Bagalini et al. [21] conducted a TRNSYS simulation of a 3 kWp grid-connected PV installation with 14.4 kWh battery capacity with economic analysis and optimized battery size to 2 kWh/kWp of PV. Battery sizing was price-limited in the past, however, the increasing number of electric vehicles sets a new challenging landscape: A high performance useable battery capacity becomes available (at different times) at home and at the workplace. In particular, the battery capacity of several employees' EVs at the workplace's parking lot may support large PV installations. Sorensen et al. [22] presented typologies of charging habits, load profiles, and flexibility potentials of EV charging in apartment buildings with multiple EV charging lots. This study exploited field data from 6878 charging sessions, employing 97 users. In these studies, EV charging mainly took place between 2 to 6 am during the night. With regards to the sizing of system's components, several works in the literature have studied the methodologies for sizing hybrid power generation in accordance with the application of different dispatch control strategies [23]. Despite the significant efforts that have been reported in the literature, the exploitation of the aggregate storage of a significant number of electric cars in a building's smart network deserves more attention, especially the effect of allowing the EV batteries to discharge energy into the building's grid must be assessed and rationally priced. As a first step in this direction, it is important to assess an optimal comparative sizing of the building's electricity consumption, the electric cars' consumption, and aggregate storage capacity and the rooftop PV panels' production capacity.

The present study explores the interaction of a large size PV system with the energy systems of a commercial building, including the battery storage from the employees' EVs. A nearly zero energy office building is studied, (currently under construction) that is equipped with a large array of rooftop PV panels, corresponding to the maximum that are allowable by its flat roof's dimensions. The building's heating, ventilation, and air conditioning (HVAC) system is fully electrified, based on a high efficiency ground-source heat pump system. Under the specific circumstances, the building becomes a net exporter to the grid. Moreover, half of the available parking places in the buildings' basement (40 places) are designed to be equipped with chargers (to provide EV charging lots). This situation makes available a significant aggregate size of battery capacity which is employed for optimal use by the building's smart grid during the working hours. Thus, the electricity surplus of the rooftop PV in sunny days is employed to charge the employees' EVs. On the other hand, high levels of battery capacity in several connected EVs may be profitably exploited to cover building's electricity loads during cloudy days or exporting electricity to the grid at peak demand hours.

2. Materials and Methods

The feasibility of operating a micro-grid on a NZEB building which is currently under construction, is investigated by TRNSYS building and energy systems simulation. The detailed transient simulation of the building shell and energy systems is routinely applied to understand and optimize the building's interaction with the system load curves. Simulations of the "typical day operation" type are carried out [24], usually focusing on specific components, such as the air-source heat pumps [25] or ground-coupled heat pumps [26]. These studies support the optimal sizing of components, assess the effect of climatic conditions, operating schedules, and controls [27]. The modular structure of TRNSYS models complex energy systems by breaking them into smaller components [28]. Building input data and component interactions are conveniently entered by means of a graphical user interface. The simulation engine solves the system of equations resulting from the component models and their interconnections. Numerous components and routines for weather data and forcing functions are included in the TRNSYS library. The

performance of this software against test results for ground-source heat pump simulations is demonstrated in [29]. The comparative performance of TRNSYS against other standardized building energy simulation software is discussed in [30]. Moreover, TRNSYS is among the certified building energy analysis software packages conforming to ANSI/ASHRAE Standard 140-2001 [31]. Since this study is based on building energy simulation results, it is important to describe in this section, the structure of the various sub-systems' models that were employed in the transient simulation, as well as the building's details and schedules and the specific scenarios of availability of the employees' EVs in the building's internal grid. The sizing of the various energy system's components in the building has been decided according to the following reasoning: the building has been designed as a NZEB, with fully electrified HVAC system that is based on a high efficiency, ground-source heat pump. Since the building has a flat roof, the maximum available space is considered to be covered by PV panels of the best available technology. Thus, the only component that needs to be sized is the number of electric cars that are connected daily to the building's charging lots. The basic assumption on this issue is that half the available parking places in the building's basement are daily occupied by employees' EVs that are bi-directionally connected to the internal grid.

2.1. Building Simulation Details

The office building that is being studied (Figure 1) has a coverage (ground trace) of 1340 m² corresponding to main external dimensions 84 m × 16 m. It has 4 stories with office spaces and meeting rooms plus a ground floor with a reception space, auditorium, and meeting rooms. The maximum number of occupants during the weekdays reaches 150 (employees plus visitors). The normal number of employees per regular office (Figure 1) are two. The parking in the basement has 80 places, out of which 40 places have been designed as dedicated charging lots for electric vehicles. As such they are equipped with 7 kW, 3-phase, 32 A/400 V chargers.

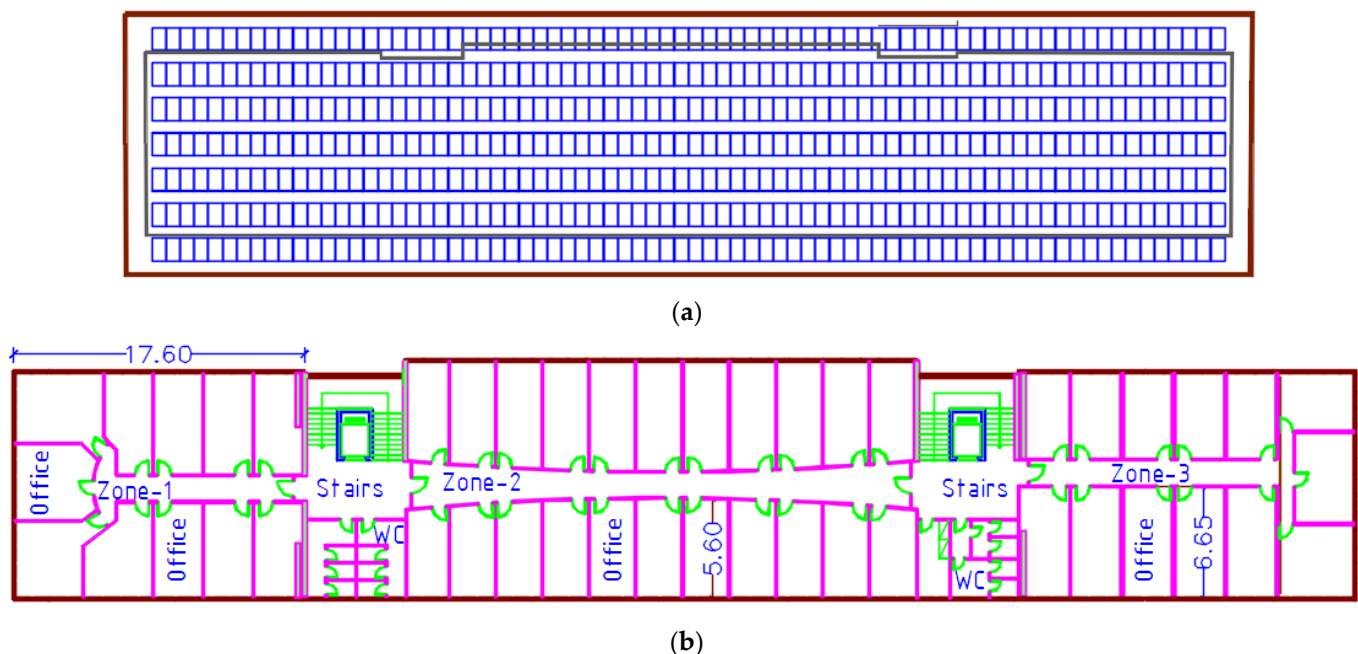


Figure 1. Cont.

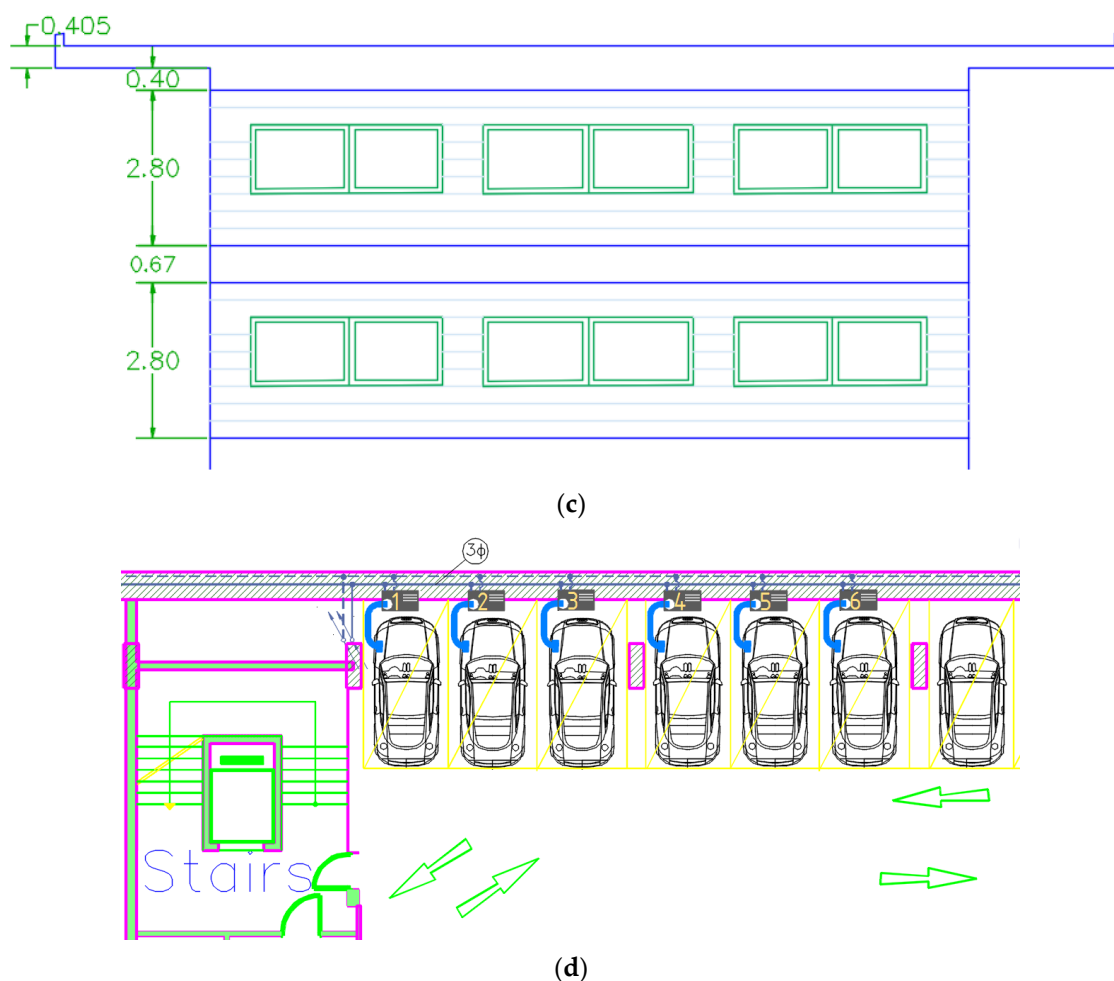


Figure 1. Layout drawing of the house that was employed in the simulations: (a) Plan of a typical floor level, (b) plan of rooftop PV installation, (c) eastward view of the third and fourth levels, and (d) part of the EV car parking places with chargers # 1 to 6 at the building's basement. Dimensions in meters (m).

This is an NZEB, an 18-zone building with a very well insulated building shell (insulation data in Table 1), energy efficient windows (low-e), and automatic shading devices for the summer, to keep cooling loads at only a little higher levels than the winter heating loads. The total floor area of the building is 6700 m² out of which the conditioned zones area is 5750 m². The ceiling height is 3 m for all levels above ground. The basement with a ceiling height of 6 m is the parking place and electromechanical installations.

Table 1. Values of the de Soto model's parameters.

Parameter	$I_{L,ref}$	$I_{0,ref}$	R_S	R_{SH}	α
Value	9.705 A	0.2991 nA	0.06054 Ω	5000 Ω	2.664

The level roof has a south facing rooftop PV installation at 20 degrees tilt angle. A total of $(78 \times 7) = 546$ panels facing SSW. The panel dimensions are 1048 \times 1765 mm. They are placed in portrait orientation in 7 series of 78 panels each. Each PV panel has 375 Wp nominal output [32], resulting in a total of 204.75 kW peak.

A plan view of the rooftop PV panels (546 panels in total, with minimal shading effects) is shown in Figure 1. Climatic data are introduced by means of a typical meteorological year (TMY) for the city of Volos. This includes the hourly input values of ambient tempera-

ture (DB), relative humidity, wind direction/speed, and the total/direct solar horizontal radiation for the full year (8760 h).

2.2. HVAC System Details and Submodels

Space heating and cooling of the building is furnished by a 210 kW nominal capacity water–water heat pump (technical data in Table A2—Appendix A). The heat pump operates as a ground-source heat pump (GSHP), exploiting a ground network consisting of 80 boreholes, $\varnothing 200$ mm \times 80 m depth each. The heat pump produces 210 kW of heating at standard ambient conditions of 7 °C, and 195 kW for cooling at standard ambient conditions of 35 °C DB. The heat pump is connected to fan coil units inside each office and air ducts in larger spaces. Space ventilation air is supplied by air ducts. Efficient lighting by use of LED lighting and high efficiency (A+) electrical equipment are considered. The modeling of the water–water heat pump is based on Type 668 [33]. The year-round heat transfer performance of the vertical U-tube ground heat exchangers loop is modeled based on Type 557a [33].

2.3. Electric Car Consumption and Performance Data

The electricity consumption of EVs lies in the range 130–260 Wh/km, depending on the vehicle speed and ambient temperature, with city driving at warm temperatures producing the lowest consumption figures. The battery charging task for 40 employees' EVs during the weekdays is assumed to be completely fulfilled by the EV charging lots: This corresponds to a daily trip of city driving to the workplace plus an equivalent distance that was covered for the rest of the daily transportation needs, assumed to be 50 km for 22 working days, or 1100 km/month, with an average consumption of 190 Wh/km (at the building's level—which includes the charging losses). The cars' needs during the weekends are assumed to be covered by charging at home or public charging stations. The total requirements for the 40 cars amount to 100,000 kWh, or about 210 kWh/month for each EV. The charging lots in the basement are equipped with forty level 2, 7.1 kW, 3-phase chargers, each of which can fully charge a large EV's 82 kWh battery in 11 h [25].

2.4. Batteries Simulation Details—Dispatch Strategy

The accurate estimation of the state of charge, capacity, and power fade analysis of Li-Ion batteries is a subject of intensive research. Various battery modeling approaches for electric vehicle simulations are described in [34]. On the other hand, the specific modeling approaches for the computation of battery state of charge are discussed in [35]. In the present study, a generic battery model from the TRNSYS library is used, relating battery voltage, current, and state of charge. It is based on Hyman (modified Shepherd) equations, with power as input [36]. A constant value of 0.9 is assumed for the charging efficiency for simplicity (charging efficiency is known to reduce for very high state of charge). With regards to the battery capacity dispatch strategy, popular control strategies in hybrid renewable energy systems include load following, cycle charging, or combinations thereof [23]. In the specific case that was studied, the role of the conventional generator is played by the external grid. The low limit of battery fractional state of charge is set to 0.30 and the charge to discharge limit is set to 0.50 at the inverter's control unit regulating the output from the rooftop PV installation. Thus, as long as battery state of charge is below 0.50, first priority is given to recharging the battery with any available PV array output, rather than sending the PV output to cover the building's electrical loads. The flowchart of Figure 2 summarizes the dispatch logic and constraints that were employed.

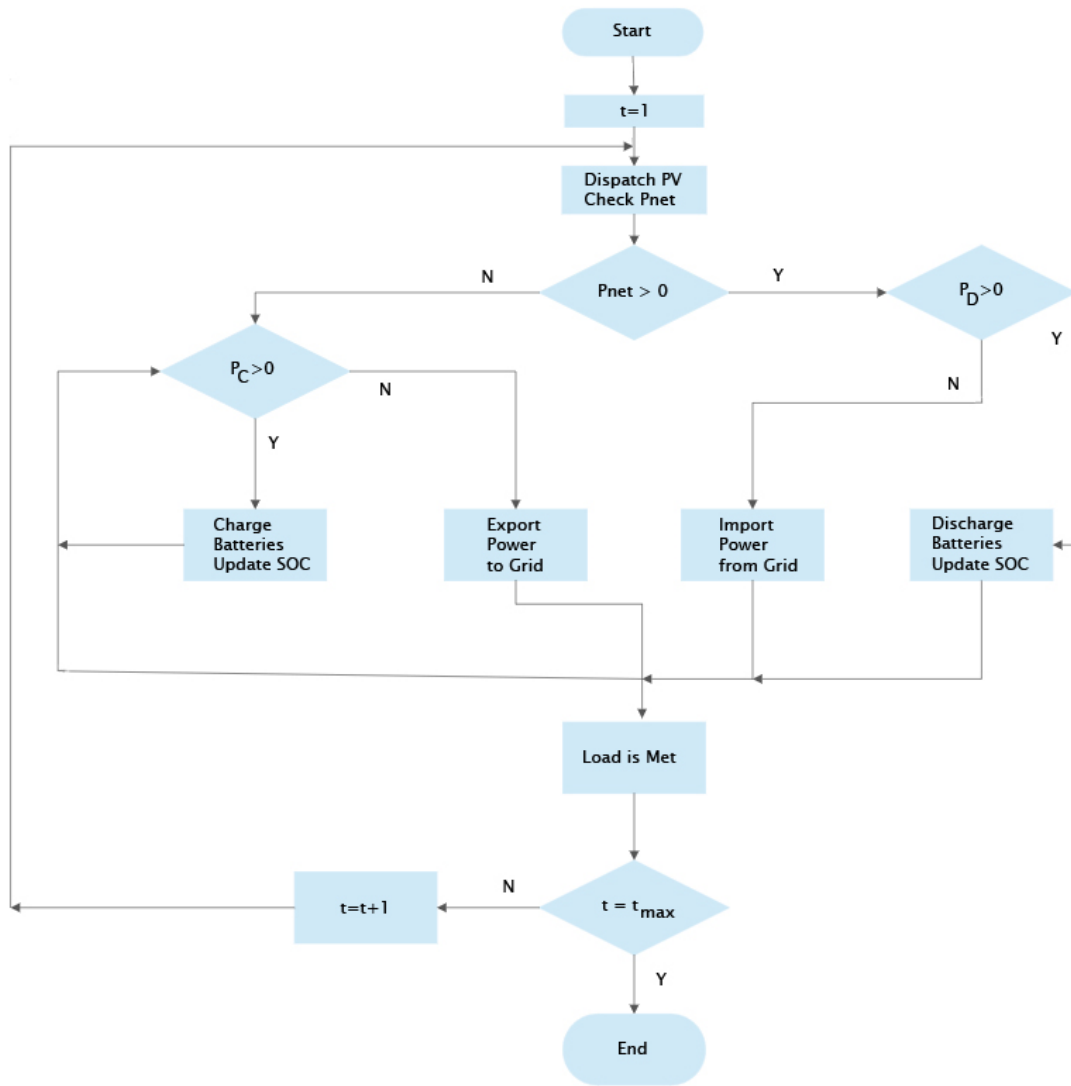


Figure 2. Flowchart of dispatch logic of the different power sources.

The available charge power (P_C) and discharge power (P_D) of the battery storage depends on its state of charge at a specified time (Soc_t), which is defined as the ratio between the remaining capacity at that time ($E_{bat,t}$) to the maximum capacity (E_{bat}) of the battery [37]. The discharge power of a battery is also affected by the C-rate. It is a measure of the power that can be discharged in one hour relative to the maximum capacity and is assumed to be 1-C. Other than Soc and C-rate, the maximum discharge power also depends on the minimum Soc (Soc_{min}) that must be maintained in the battery:

$$Soc_t = \frac{E_{bat,t}}{E_{bat}} \times 100\% \quad (1)$$

$$P_C = (1 - Soc_t) \frac{E_{bat}}{1h} \quad (2)$$

$$P_D = (Soc_t - Soc_{min}) \frac{E_{bat}}{1h} \quad (3)$$

where Soc_t and Soc_{min} are in percentages, E_{bat} is in kWh, P_C , and P_D are in kW. The power generation system in this case consists of the variable generation PV array, the EV Battery storage, and the (positive or negative) import (or export) to the external grid. Each of these power generations is dispatched sequentially to meet the building's electricity load, depending on the selected dispatch strategy so that the unmet load is equal to zero. First,

the PV generated power is dispatched. The resulting net required load P_{net} (kW) is given by the following relations:

$$P_{\text{net}} = P_{\text{req}} - P_{\text{pv}}^* \quad (4)$$

$$P_{\text{pv}}^* = \eta_{\text{pv,inv}} P_{\text{pv,dc}} \quad (5)$$

where P_{req} is the required load (kW), P_{pv}^* is the PV system's generation (kW), $\eta_{\text{pv,inv}}$ is the PV inverter's efficiency (%), and $P_{\text{pv,dc}}$ is the DC power that is generated by the PV array (kW). The value of the net required load can be zero, negative, or positive. Zero value indicates that the required load is satisfied precisely by the PV array. A negative value means excess power that is produced by the PV system, which can be employed to charge the battery if the battery Soc is <1 . Otherwise, the excess power is exported to the network. On the other hand, a positive value would imply that there exists an additional load to be met, either by discharging the battery, if $\text{Soc} > 0.3$ and batteries are connected, or by electricity import from the external network.

The battery's power set point (P_{bat}^*) in kW is determined as follows:

$$P_{\text{bat}}^* = \begin{cases} 0 & \text{if } P_{\text{net}} = 0 \\ -\min\left(P_D, \frac{P_{\text{net}}}{\eta_{\text{binv}}}\right) & \text{if } P_{\text{net}} > 0 \\ -\min\left(P_C, \eta_{\text{brec}} P_{\text{net}}\right) & \text{if } P_{\text{net}} < 0 \end{cases} \quad (6)$$

where η_{binv} and η_{brec} are the efficiency of the battery's inverter and rectifier (%), respectively. P_{bat}^* is negative if the battery is discharged and positive if the battery is charged. The power that is imported from the grid (P_{grid}^*) in kW is determined by the unmet load and the power to charge the battery, and compared it with the maximum permissible rate of the imported power:

$$P_{\text{grid}}^* = \min\left(P_{\text{grid,rate}}, \left(P_{\text{net}} + \frac{P_C}{\eta_{\text{brec}}}\right)\right) \quad (7)$$

Whenever P_{grid}^* takes negative values, electricity is exported to the grid.

The following additional assumptions are made for battery charging rules and schedules:

- (i) An average of 40 car batteries stay connected to the building's smart network via the EV chargers, between 9:00 and 17:00 on workdays. The maximum allowable power for battery charging 160 kW.
- (ii) Very few (1–2) car batteries are connected on Saturdays and Sundays. That is, almost no charging of the batteries is allowed by the building's smart grid during the weekends. Discharging during electric car trips in weekends is assumed to be fully compensated by outside charging.
- (iii) While staying connected at the parking lot, the EV batteries are mainly charged by the PV inverter. Under normal conditions, no charging is done with power from the grid.
- (iv) During the working hours, the EV batteries are allowed to discharge whenever necessary in order to cover the buildings electrical loads during cloudy days of peaks. The maximum allowed power during discharging is set at 50 kW.
- (v) Discharging of the batteries for car motion is assumed to occur during the night (cars not connected to the building's grid).

2.5. Photovoltaic System Submodel

The available information in the technical data sheets [32] does not allow detailed PV operation modeling. The original model by De Soto et al. [38] reconstructs a PV module's operating curves by fitting basic manufacturer's data. The cell is modeled as an equivalent one-diode circuit with five main parameters describing its operation: I_L (the light current), I_0 (reverse diode current), R_S (module series resistance), R_{SH} (shunt resistance),

and α (modified ideality factor). The panel's I–V curve characteristics are produced by the equation:

$$I = I_L - I_0 \left(e^{\frac{V+IR_S}{\alpha}} - 1 \right) - \frac{V + IR_S}{R_{SH}} \quad (8)$$

where the modified ideality factor α depends on the cell temperature T_C , the number of cells in series N_S , the usual ideality factor η_I , Boltzmann constant k , and electron charge q :

$$a = \frac{N_S \eta_I k T_C}{q} \quad (9)$$

By inserting the standardized pairs of I–V values that are provided in the data sheet [32], these equations are solved for different reference conditions, by means of an EES plugin for Type 194, producing the following parameter values (Table 1).

The size of the rooftop PV panels are arranged in portrait orientation as shown in Figure 1. The panel dimensions are 1048 × 1765 mm and nominal output is 375 Wp (technical data in Table 2).

Table 2. Technical data of the 375 Wp monocrystalline silicon, 120 half-cells PV panels NU JC375 [32], as used in type194.

PV Module Parameter	Value	Comments
I_{SC} at STC	11.62 A	Short circuit current
V_{OC} at STC	41.08 V	Open circuit voltage
I_{MPP} at STC	10.83 A	Current at max power point
V_{MPP} at STC	34.63 V	Voltage at max power point
Temp. coefficient of I_{SC} (STC)	0.057%/K	α_{ISC}
Temp. coefficient of V_{OC} (STC)	−0.263%/K	β_{VOC}
Number of cells wired in series	2 strings × 60	modules
Module temperature at NOCT	318 K	
Ambient temperature at NOCT	293 K	
Module area	1.85 m ²	
Module efficiency	20.27%	

2.6. TRNSYS Types and Simulation Details

The system model in the TRNSYS simulation environment is anchored on an 18-zone model of the office building (Type 56). The rooftop PV installation is included and an average of forty EVs' batteries are connected to the grid whenever the cars stay at the Company's charging parking lots. In addition to the standard utility components of the TRNSYS environment (Type 54—weather generator, Type 16—Solar radiation processor, Type 69—effective sky temperature, Type 501—ground temperature calculation, and Type 33—psychrometrics), specific TRNSYS component models for the rooftop PV panels (Type 194), the inverter (Type 48b), the car batteries (Type 47c), the water–water heat pump (Type 668), and the ground heat exchangers' loop (Type 557a) are employed in the simulations. The specific subroutines belong to the TRNSYS and TESS libraries [33].

Having described in a concise manner in this section, the modeling approach for the building, its energy system and electric cars' battery charging and discharging behaviour, the useful results on the systems' operation and interaction are presented and discussed in the next section.

3. Results

The transient evolution, with 0.1 h as time step of the following variables, is selected to be presented in the simulation results, to describe the electrical system's behavior:

Battery state of charge: The aggregate battery capacity (i.e., refers to the sum of the average forty batteries' state of charge).

Power from grid: The electric power that is imported from the grid whenever the batteries cannot cover the building's (and EVs') electricity needs.

Power surplus (for EV charging or for exportation to the grid): The difference between electric power that is produced and consumed by the building's HVAC system, lighting and electric appliances. This is managed by the smart network and maybe employed for the charging of employees' EVs or exported to the electricity grid.

Power that is exported to the grid: After subtraction of the electric power that is consumed for the aggregate EV battery charging, the remaining power is exported to the grid.

3.1. Monthly System's Performance and Annual Summary

The system's performance is better assessed by the building's monthly energy data. Figure 3 presents the evolution of the rooftop PV monthly electricity production. The highest production is observed in June and July, exceeding 46,000 and 47,000 kWh/month, respectively, and the lowest is observed at around 12,000 kWh in December.

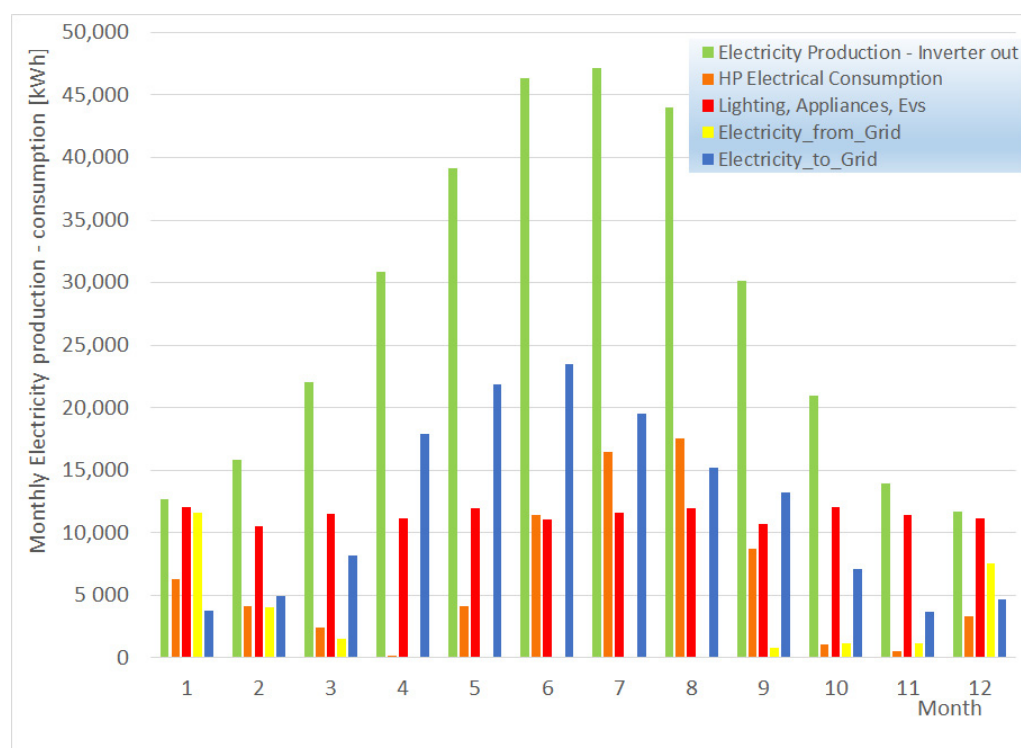


Figure 3. Monthly electricity production and consumption during one full year (car charging included).

The electricity consumption of the heat pump (to be examined in more detail in Figure 4) is variable throughout the year. However, it becomes negligible during the neutral months. The office building's electricity consumption for the lighting and electrical appliances averages to less than 3000 kWh/month. The total annual electricity consumption of the building is predicted to the amount of 112,000 kWh, or about 20 kWh/m²y. Now, the total annual electricity that is produced by the PV installation is predicted at 336,000 kWh. Before exporting the surplus quantity to the grid, it is interesting to see if there is a possible outlet inside the building's smart grid. Starting with the employees' EVs, the charging of the 40 electric cars during the week days consumes 380 kWh per working day (8400 kWh/month). This amounts to 101,000 kWh/year, which is about 30% of the total PV electricity production. Selling this quantity to the employees which are owners of electric cars can be beneficial to the building, because the charging period coincides with the hours of sunshine. This option will be examined in more detail next.

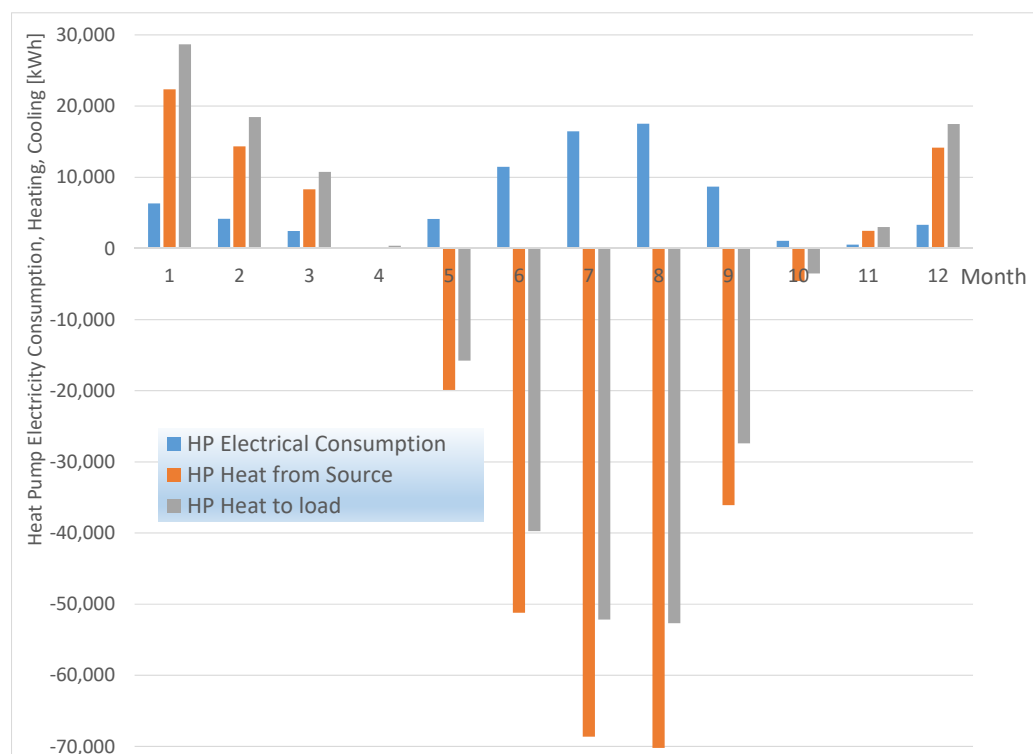


Figure 4. Monthly summaries of heat pump electricity consumption, heat from source, and heat to load. Cooling mode prevails during the months of May to October, as seen by the negative (cooling) kWh.

Overall, the specific rooftop PV installation size results to a near zero-energy building, which is a net exporter of electricity to the network. Electricity imports maximize at 11,500 kWh in January, because of the fact that the batteries are assumed to start at zero charging levels. Thus, imports during February reduce to 4000 kWh and further reduce to 1500 kWh during March. The building starts to import again small quantities of the order of 1000 kWh during September, October, and November. Finally, imports during December reach 8500 kWh. The rooftop PV installation is optimized for maximum production during the summer months, because of the 20° panels' tilt angle. Thus, the monthly electricity exports to the grid significantly exceed the respective imports (whenever they exist) for all months except for December and January.

The monthly electricity consumption of the ground-source heat pump during the year is presented in Figure 4. It should be noted here that the actual operation of ground-source heat pumps may deviate significantly from the theoretical design predictions [39]. This is mainly due to the uncertainty regarding the ground thermal properties along the different layers of the boreholes [40]. Another important uncertainty factor is the year-round variation in soil and ground humidity along the boreholes' depth [41]. The seasonal heating and cooling production and coefficient of performance (COP) on a monthly basis, is also presented. The monthly average COP during winter varies between 4.4 and 5.6. On the other hand, the monthly average COP during the cooling season varies in the range 3.2–4.0. The summer cooling loads are considerably higher than the winter heating loads. This is an effect of the prevailing weather conditions on the site, with mild winters and summer heat wave episodes. The annual heat pump's electricity consumption reaches 76,300 kWh, (13 kWh/m²y). This is a very low consumption that becomes attainable by the building's shell insulation specifications and the ground-source heat pump's efficiency levels. The electricity consumption of the ground-source heat pump reduces to 170 kWh during the neutral month of April, and reaches only 1000 and 500 kWh during October and November, respectively.

Figure 5 gives an overview of the electricity self-consumption of the office building, including the charging of the 40 employees' EVs during weekdays, compared with the rooftop PV production. The monthly variation of non-renewable electrical power consumption of all Greece for the period 1 July 2021–30 June 2022 is depicted on the same Figure. A significant electricity surplus is observed from April to October. The comparison with the electricity needs of the country indicates that exportation to the grid is welcome for all months. However, it is essential to study the specific hours that electricity would be available (and welcome from the grid) for exportation.



Figure 5. Monthly variation of PV electricity production, electricity consumption of the office building, and charging requirements for the 40 employees' electric cars, compared to the trend in the non-renewable monthly electricity consumption of Greece during 2021–22.

Although the absolute maximum of non-renewable electricity load of 3000 GWh is observed again in July and August, the non-renewable demand never drops below 1500 GWh on a monthly basis. Thus, the maximization of the building's electricity surplus for June coincides with a high monthly consumption profile for the country. Ideally, the same high quantity of electricity would be welcome also for July and August. According to Figure 5, a reduction in the available electricity for exportation to the grid is observed for July and August due to the increase of the cooling loads. Nevertheless, the available quantities remain higher than 115,000 kWh for these two months where the exportation to the grid remains highly beneficial, at least as integral quantities. Moreover, the buffering effect of the added electric car batteries leads to synergies that will be discussed in detail in the next section, in terms of the transient system's performance.

3.2. Hourly System's Performance and Interactions

As a next step, the transient energy system's performance is presented and discussed.

A typical daily electricity demand curve of the Greek system during a cold, sunny winter day is presented in Figure 6. For comparison, the respective demand curve for Sunday is presented to highlight the different profiles between a weekday and a weekend day in the same period. During the cold, sunny weekday, the first characteristic peak

(morning peak) at 7.15 GW is significantly higher than the evening peak. Following the subtraction of the hourly PV generation in Greece during the specific day, the two peaks for non-PV electricity load are seen to be of equal magnitude (5.5 GW). Of course, the evening peak is significantly steeper. This evening ramp would require a flexible power source of 550 MW to be added during the three-hour period 17:00–20:00.

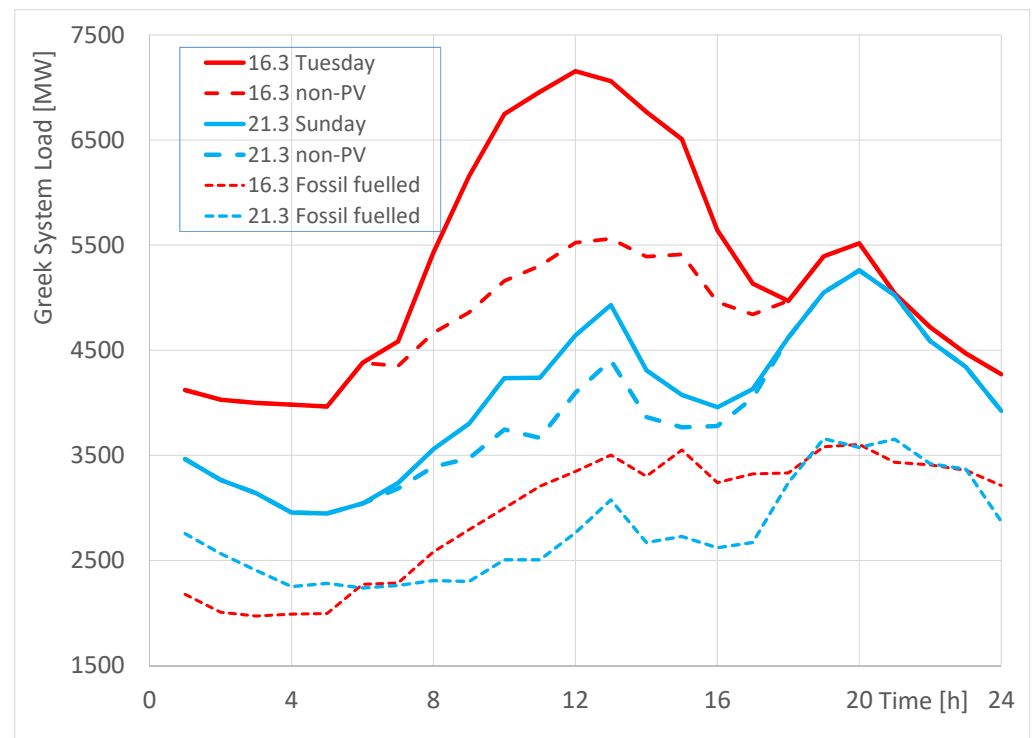


Figure 6. Daily variation of the Greek system electricity load curve during a week-day and a weekend day (Sunday) with low ambient temperatures and clear skies, in winter 2021. For comparison, the respective load curves without the contribution from PV parks is drawn in the same Figure [42].

Obviously, the batteries of electric cars that are connected to the building's smart network are not allowed to assist by exporting electricity by the assumed dispatch logic, since no PV capacity is available by that time. On the other hand, significant battery capacity may remain available for exportation to the network in order to assist in meeting the morning ramp.

Figure 7 presents the transient simulation results for the first week of the typical meteorological year (assumed to start on Monday). The heated zones of the building are kept at 20 °C, except for the Saturdays and Sundays, as seen by the example of Zone 1 at the building's ground floor (see Figure 1).

The batteries' aggregate is assumed to start empty at the first day of the year, for simplicity. The batteries are seen to charge quickly during the first, third, fourth, and fifth days of this week, eventually reaching 50% of their capacity, assumed to keep it during the weekend. The batteries are not allowed to discharge as long as they stay below the 30% FSC threshold. During the second week (Figure 8) they are allowed to discharge by the dispatch logic, to meet the demands of the heat pump, lighting, and electrical appliances. The batteries are discharging also during non-working hours, whenever each car is in motion, provided that they have exceeded the 30% threshold.

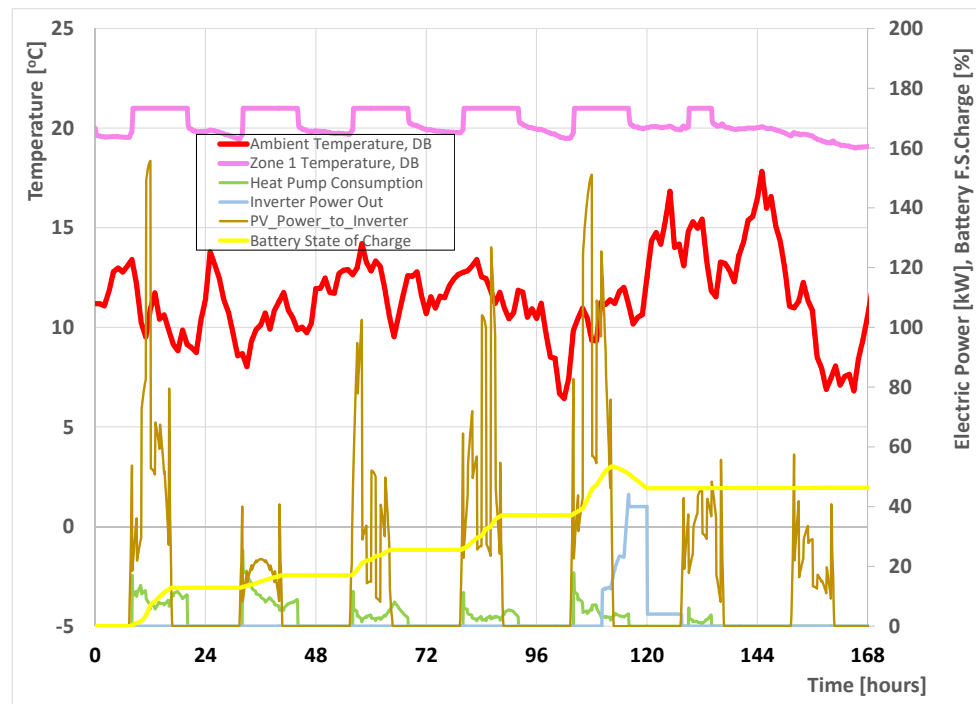


Figure 7. Ambient temperature, room temperature, heat pump electricity consumption, and PV inverter's outlet power in the first week of January. The conditioned zone temperatures are kept at the setpoint of 20 °C as seen by the example of Zone 1. The batteries, assumed to start from zero charging levels, reached 50% of their total aggregate capacity, since all the building's needs are covered by importing electricity from the grid.

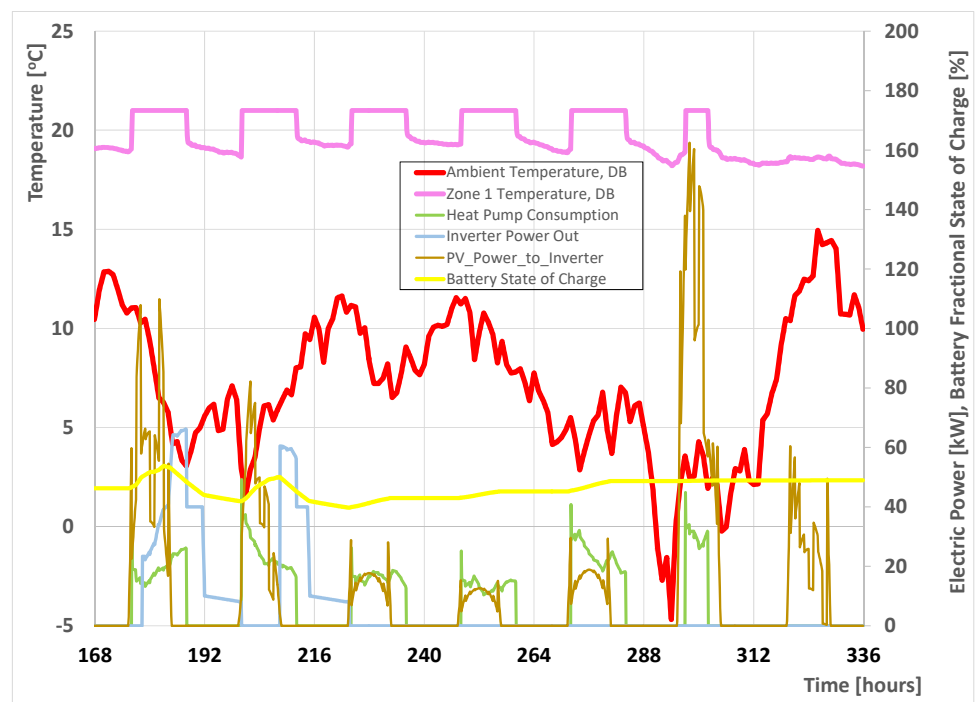


Figure 8. Ambient temperature, room temperature, heat pump electricity consumption, and PV inverter out power in the second week of January. The batteries have reached 50% of their total aggregate capacity and start to discharge during Monday and Tuesday, to cover the building's loads and electric cars' consumption. During Wednesday to Friday, the little available PV electricity is employed with first priority to charge the batteries, until they reach 50% FSC.

A more detailed study of the transient system's behavior can be done in the example of Figure 9, which concerns a cold, sunny day of March. This day is selected to correspond to the typology of Figure 6. The battery state of charge is starting higher than 98% FSC. The battery is charging slowly to 99% during the day by the surplus electricity that is provided by the PV panels, which exceeds the heat pump, lighting, and electrical appliances consumption.

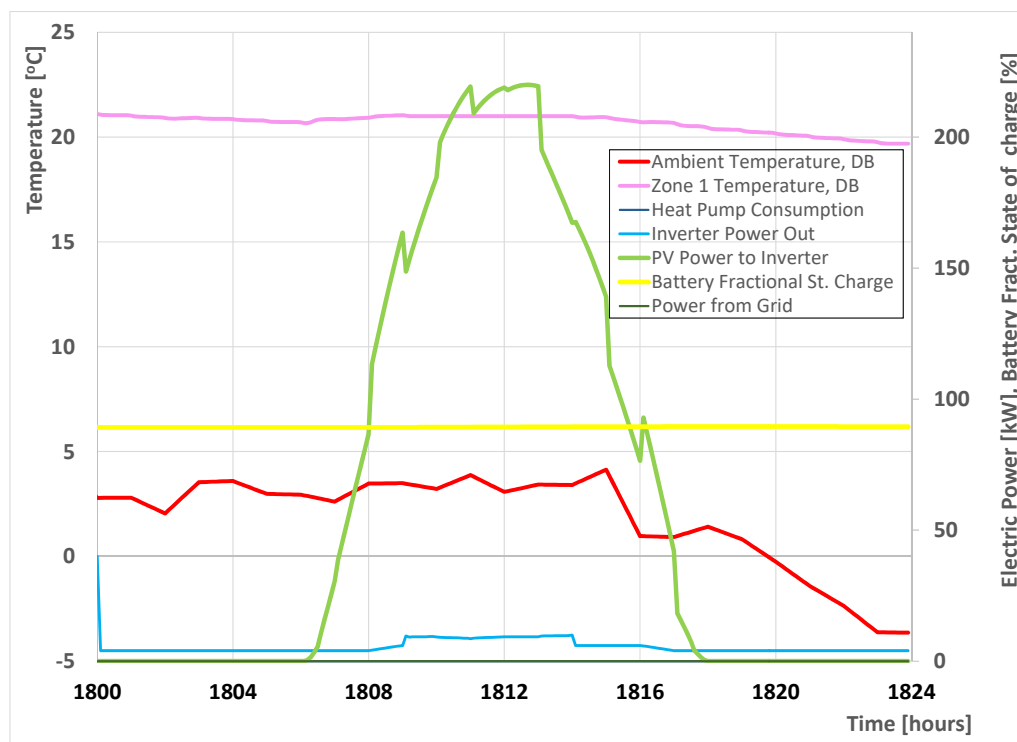


Figure 9. Ambient temperature, room temperature, heat pump electricity consumption, and electric power at the PV inverter outlet, during a cold, sunny weekday of March, starting at midnight.

Next, the Greek system electricity load curve in a typical weekday of late April 2021, is presented in Figure 10. As expected for a weekday, the morning peak is higher than the evening peak. However, when the PV generation is excluded, the evening peak to be covered by non-PV power generation is significantly higher, at 6.5 GW. The evening ramp becomes more enhanced, requiring a flexible 400 MW power source to be added each hour between 17:00 and 20:00 (a total of 1.25 GW to be added in 3 h). The margin for increasing the installed PV capacity is significant: the system exploits 3.5 GW of fossil electricity during the 24-h period, with a major part thereof fueled by natural gas.

Figure 11 presents the simulated transient energy system's operation during a similar season (first days of May) for comparison. Most part of April and the beginning of May usually correspond to the spring neutral season. Thus, no more heating is necessary, the temperature set point is shifted to cooling mode. The onset of cooling operation is observed on Monday, Tuesday, and Wednesday at noon. The batteries are charged up to 100% capacity during sunny days. They become fully charged during the day and easily cover the afternoon working hours' loads by discharging, making the building self-sufficient, including the EVs electricity consumption. Moreover, electricity becomes available also for export to the grid during certain hours of the day, as indicated below.

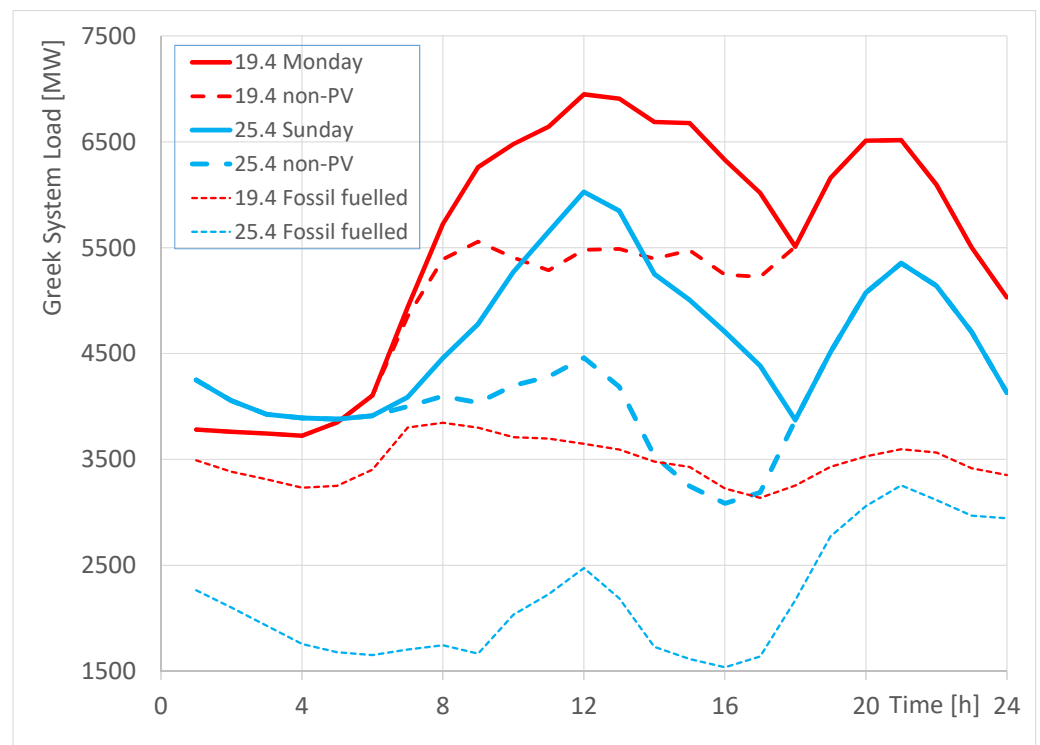


Figure 10. Greek system electricity load curve during a week-day and a weekend day (Sunday) with normal ambient temperatures and clear skies, in April 2021. For comparison, the load that is covered without the PV contribution, and the fossil-fuelled load are shown [42].

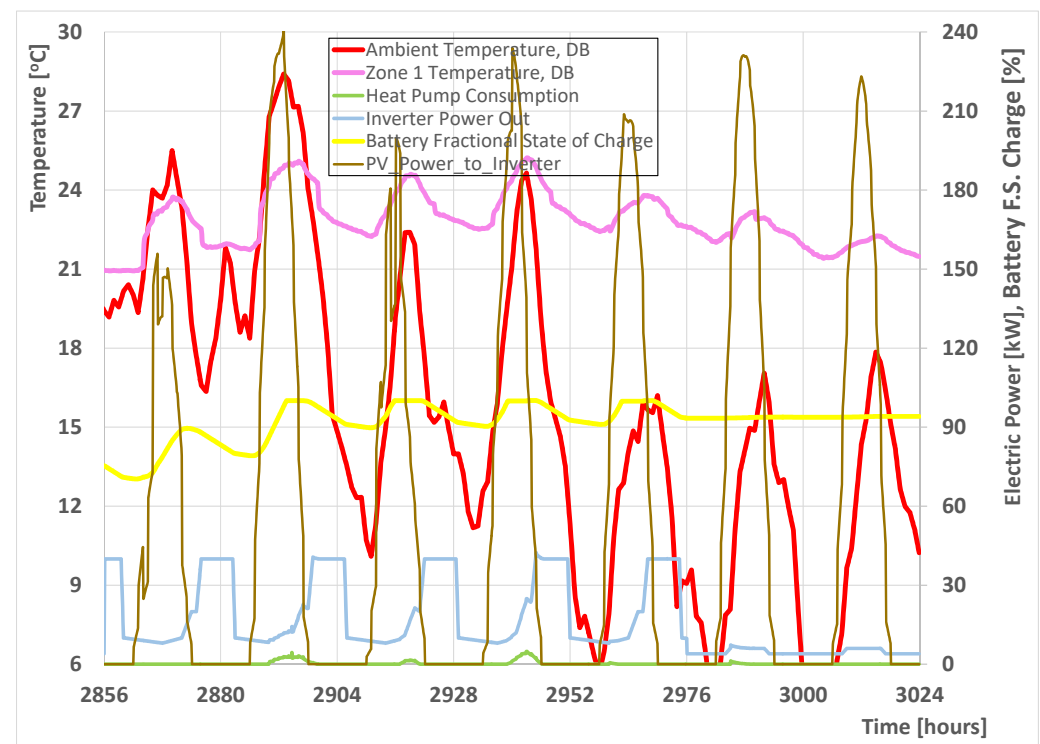


Figure 11. System's performance during a week in the beginning of May. The temperature set point to 25 °C for the cooling season, however, the heat pump is only slightly necessary. This results in the batteries being charged up to 100% of their capacity.

The system's operation in the neutral period (late April), is presented in Figure 12 for a sunny weekday. The battery has discharged to 72% because of the reduced PV electricity production of the previous, cloudy days. The battery aggregate is quickly charging during the morning, with the PV electricity fully covering the building's loads. Small quantities of surplus electricity (about 8 kW power levels) are exported to the grid during several hours in midday. The building and EVs are seen to be completely autonomous from the electricity network.

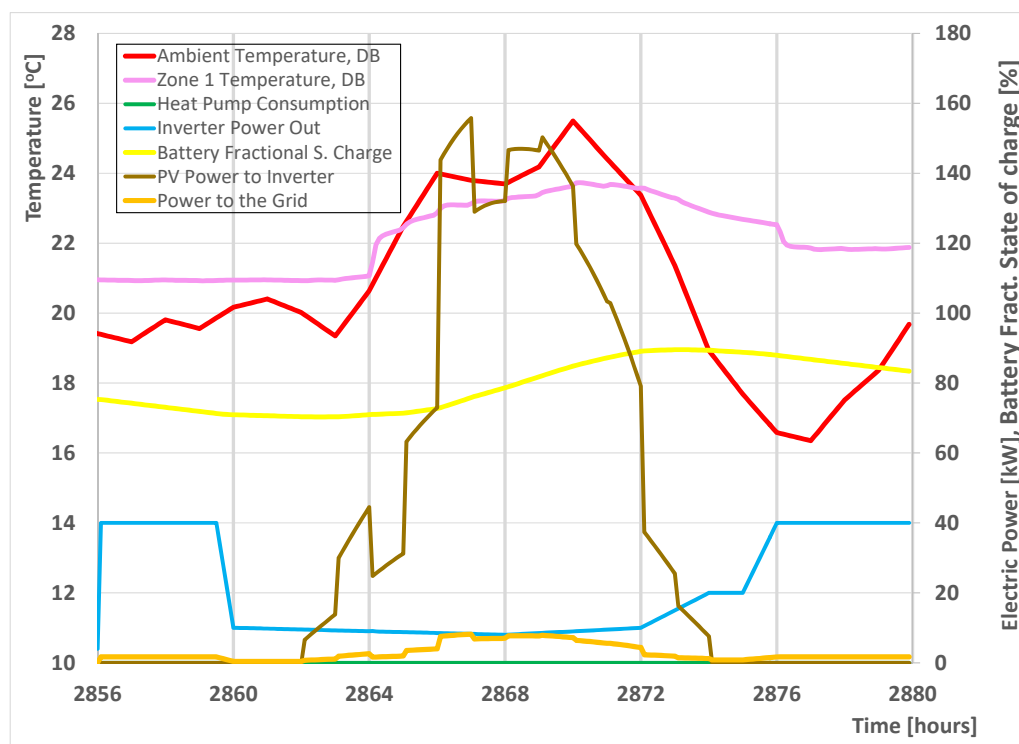


Figure 12. Ambient temperature, room temperature, heat pump electricity consumption, and PV inverter out power variation, during a sunny weekday of the end of April, starting at midnight.

A typical system's operation during the summer season is presented next. The focus is shifted to the Greek system electricity demand curve during a hot day in the end of June 2021 (Figure 13). This was a hot period with several heat waves. During the weekdays, a very high characteristic noon peak is observed, reaching 8.5 GW. This significantly exceeds the evening peak, due to the higher space cooling demand.

On the other hand, when the hourly PV generation, which is very big reaching about 1.6 GW, is subtracted, the evening peak for the non-PV load becomes higher, reaching 6.8 GW. On the other hand, the evening ramp is not very high, maximizing between 18:00 and 19:00. It requires a flexible power unit of 430 MW for just 1 h. During this hot summer season, the maximum ramp rate for the day, at about 450 GW/h is observed between the hours 05:00 and 06:00 during the morning ramp-up. This would require additional flexibility, with open cycle gas turbines or similar units. As seen in this Figure, a further increase in the installation of PV units assists the electricity grid to face the morning ramp rate with reduced flexibility. This increase in PV-installed capacity will be beneficial for all day, since the Greek system is seen to exploit high power levels ranging between 2.5 and 3.5 GW of fossil electricity during the specific 24-h period, out of which a significant part is fueled by natural gas.

Figure 14 presents, for comparison, the simulated system's operation in the first days of July. These days are similar to the ones that are presented in Figure 13. The heat pump operates frequently in cooling mode to address the high cooling loads of the successive heat waves.

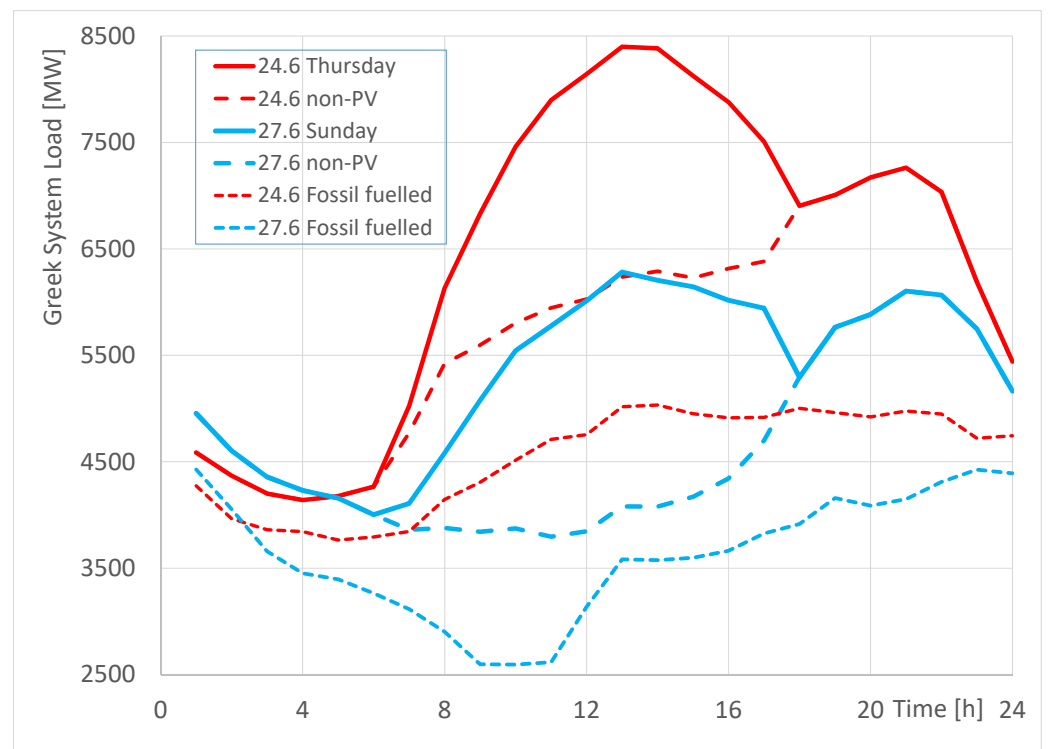


Figure 13. Greek system demand curve during a week-day with high ambient temperatures and clear skies, and a cloudy Sunday in late June 2021 (a heat wave episode recorded). The load curves without the PV contribution and the demand that are covered by fossil fuelled power plants are drawn in the same Figure [42].

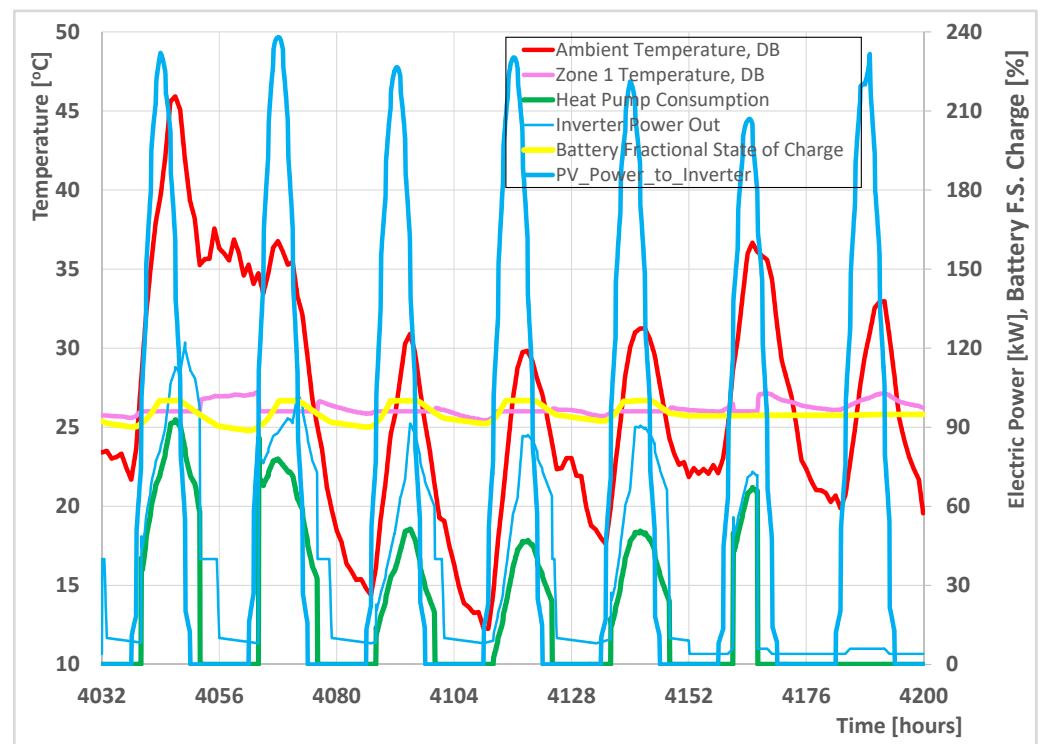


Figure 14. Transient performance of the system during one week in late June. Temperature set point to 25 °C.

Starting from 4042 h, high ambient temperatures are seen to significantly increase the operation and electricity consumption of the heat pump during the hot hours. The ground-source heat pump is very efficient in cooling operation because of the significant heat capacity of the ground boreholes. The battery aggregate constantly keeps a high state of charge levels, in the range 90–100% FSC. These levels are supported by the high production levels of the rooftop PV installation, which outperforms the house's loads and electric cars' demand. After 4080 h, the ambient temperature levels are reduced, the heat pump's consumption drops, and the battery charging levels stabilize even higher (95–100% FSC). The batteries stay fully charged during the noon hours, the house becomes again a net electricity producer and exports high levels of electric power to the grid. This is presented in Figure 15, which concerns the first day (Monday) of the specific week, which has the highest ambient temperature levels, exceeding 45 °C. The variation of power levels that are exported to the grid, peaking at 150 kW at 12:00 h and continuing at high levels until 15:00, is shown superimposed. The transient behavior of the batteries FSC may be clearly correlated to the PV production and the load profiles of the house, EVs and the heat pump. As usual, the main battery charging task is shifted to the morning hours, where plenty of PV electricity is available during the sunny days.

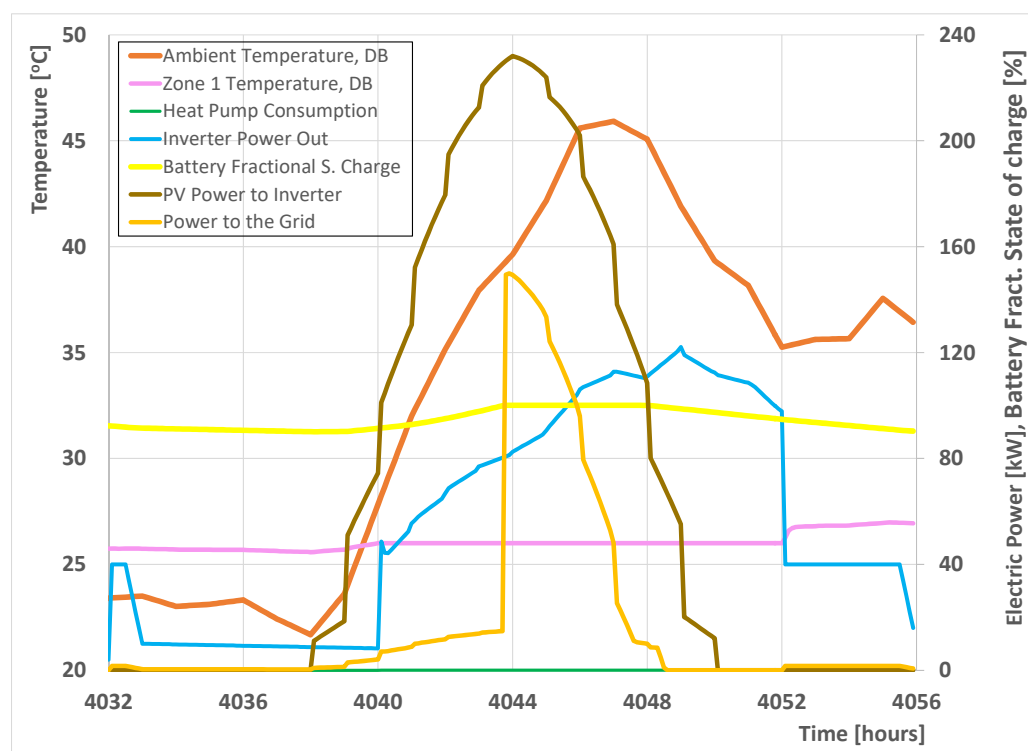


Figure 15. Ambient temperature, room temperature, heat pump electricity consumption, and PV inverter out power during a hot, sunny day in late June, starting at midnight.

Finally, Figure 16 presents the distribution of the previously computed amounts of power from the grid and the respective power that is transferred to the grid in the course of one full year and how much the peak power is transmitted to or from the network. A significant number of electricity exportation peaks are observed, some of them reaching up to 200 kW in power. As already seen in the transient simulation diagrams, (see for example Figure 15), these instances usually do not exceed the duration of 1–2 h in a day. This type of high-power intensity exports to the grid are frequent during the summer months from May to September. Export to the network occurs also during the weekends throughout the year, since no battery charging takes place and there exists a surplus of electricity, especially during sunny summer weekends. On the other hand, as seen in more

detail in Figures 12 and 15, there exists more frequent periods of electricity export at low power levels (1–5 kW), distributed all year round. The annual electricity that is exported to the grid amounts to 8220 kWh (Figure 3). On the other hand, the annual electricity that is imported from the grid is computed to the amount of 1010 kWh. As seen in Figure 16, these instances are mainly concentrated during the winter months, December to February, where the cars' batteries' charging levels are low and frequently drop to the FSC = 0.3 threshold. The grid power input levels usually peak at 50 kW during December, January, and February, seldom reaching higher power levels up to 100 kW.

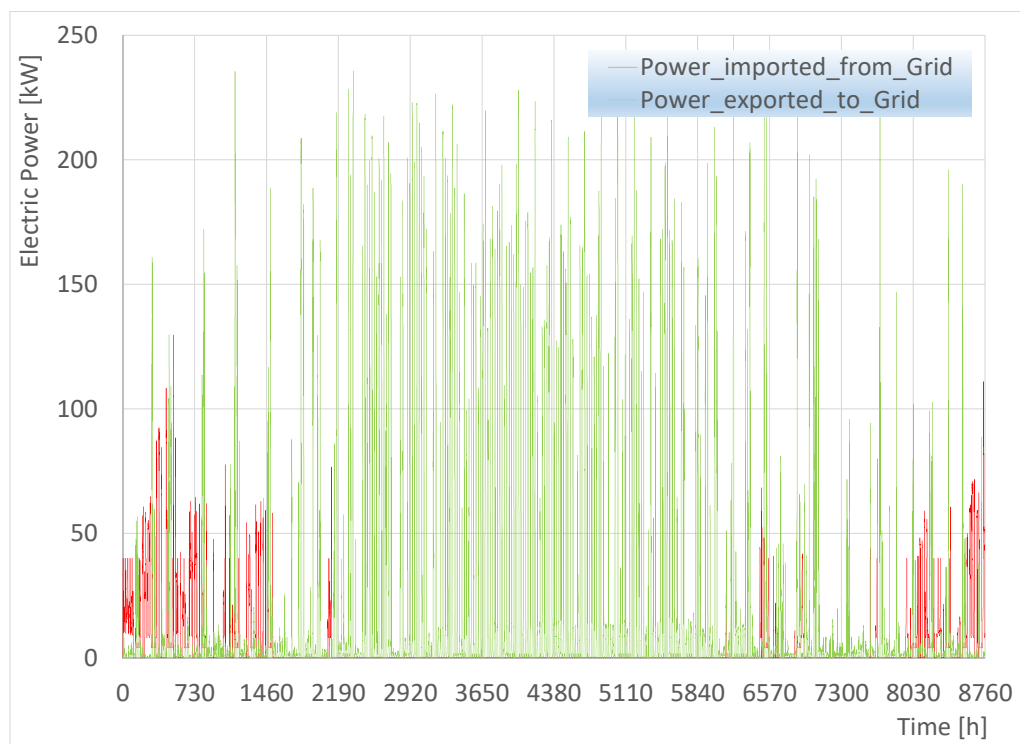


Figure 16. Power levels that were imported or exported to the electricity grid in the course of the year (charging the employees' EVs during the day).

A different view of the electricity exchange of the building with the external grid can be seen in Figure 17, where the total annual electricity flow from grid and the respective export to the grid from the building are plotted as function of the hour of day. According to this diagram, electricity imports from the grid of a significant value occur only during the morning hours 08:00–10:00 am during winter, as already presented in Figure 3. On the other hand, the bulk of electricity exports to the grid, which are an order of magnitude higher, takes place between hours 07:00 and 17:00. The maximum exported electricity occurs between 12:00 and 14:00.

Thus, the system's simulation results that are presented in this section highlight the system's performance and interaction between the building's electricity consumption, battery storage, rooftop PV production, and electricity exchange with the external grid, on a monthly, seasonal, daily, and hourly level. Once the indicative quantities of electricity exchange are assessed, the study can move forward to assess a rational means of pricing of electricity for charging the employees' EVs, compensation of the EV owners for the additional cycling of their car's battery, and pricing of the electricity that is exported to the grid according to the specific time slots in relation to the needs of the morning or afternoon ramp.

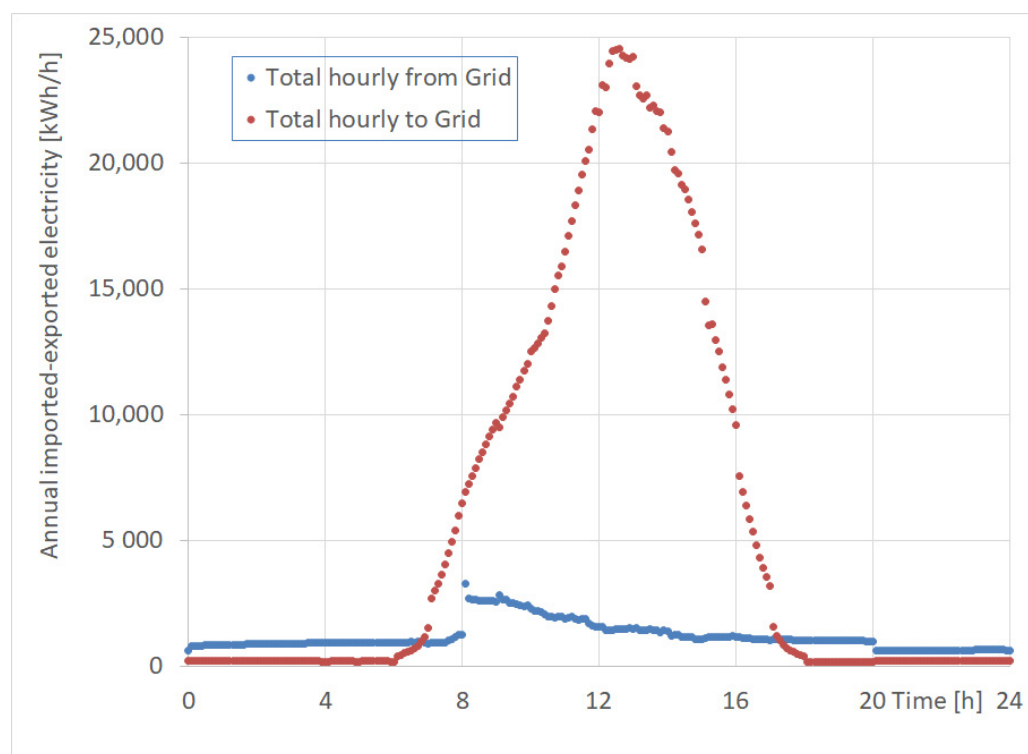


Figure 17. Total annual electricity that is imported—exported to the grid during the different hours of the day.

The results of this study indicate possible directions for the exploitation of the electricity storage capacity that is presented by the high penetration rate of electric vehicles in the fleet. According to the results that are presented here, the installation of large rooftop PV panel arrays in commercial buildings may profitably support smart grids at the building's scale, by exploiting the significant electrical storage capacity of the employees' EVs during the working hours. This trend is expected to run in parallel with the significant expansion in the installed PV capacity in Greece that is predicted in specialized studies [43]. As a next step, it will be interesting to study the economics and optimal regulation rules for smart grids to be operated in the specific type of building, and test optimal algorithms to determine the prices to be charged and the financial incentives that are offered to the employees—EV owners to allow their cars to be connected to the private network of the building. In this context, it will be interesting to exploit actual performance data by means of machine-learning methods for the prediction of battery aging as function of the number and intensity of charging-discharging cycles that are occurring during the operation of the internal electricity network [44].

4. Conclusions

Understanding the implications of introducing increasing numbers of electric vehicles on the electricity demand patterns is essential in the current, rapidly evolving financial and energy environment. The rapid electrification of the car makes available a huge aggregate storage capacity in the cars' batteries. The EV batteries may support privately operated smart grids at a commercial building level. The interaction of this storage with the building's rooftop PV installation, electrical loads, and air conditioning system's consumption, may lead to synergies and energy efficiency gains. To this end, a system's design and sizing investigation is carried out in this work, aiming to support the future implementation of a micro-grid in a NZEB office building which is currently under construction.

A transient simulation of the building's energy system, including the electricity production of the rooftop PV installation and the charging/discharging behavior of the employees'

EV batteries is performed. The interaction of these systems is depicted in the monthly operation of the building's energy system, as well as the daily and seasonal balance between the electricity that is produced, consumed, imported, and exported to the external network. The system's performance is discussed against the respective electricity demand of the Greek system in 2021–2022.

The annual electricity consumption of the building is computed to be 112,000 kWh (20 kWh/m²y). The annual workdays' electricity needs of the 40 electric cars, amounting to 101,000 kWh, can be fully met with surplus from the 336,000 kWh rooftop PV electricity production. Further, the building becomes a net exporter of electricity to the grid during specific time slots that are beneficial to the stability of the grid.

The transient simulation results bring to the foreground ways in which ways the system contributes to the stability of the network. First, it relieves the system from the charging load of the EVs during the week-days, since they are charged in-house. Second, it alleviates the EV charging load from the late afternoon—evening hours, to the morning—noon hours, thus reducing the steepness of the evening ramp of the electricity load curve.

According to the results of the simulations and the seasonal performance of the Greek system during 2021–2022, additional PV capacity would be beneficial for the system in all seasons. A significant part of this capacity could be produced by large rooftop PV installations in commercial buildings. Exploiting the increasing storage capacity of the electric vehicles reduces the necessary flexibility to be added to the grid due to the increase of variable renewables.

Author Contributions: Conceptualization, O.Z. and A.S.; methodology, O.Z. and G.S.; software validation, G.S.; formal analysis, G.S.; investigation, G.S.; writing—original draft preparation, G.S.; writing—review and editing, A.S.; project administration, O.Z. All authors have read and agreed to the published version of the manuscript.

Funding: This research received no external funding.

Acknowledgments: The authors wish to thank Aphrodite Ktena, Energy Systems Laboratory, National and Kapodistrian University of Athens, for fruitful discussions on smart micro-grids and smart charging of electric vehicles.

Conflicts of Interest: The authors declare no conflict of interest.

Appendix A

This section contains additional data on the office building's location, climate type, and building envelope characteristics and the water–water heat pump.

The building is located in Volos, a coastal city in Greece, latitude 39°21', longitude 22°56', with a warm and temperate climate, average monthly temperatures ranging between 8 and 10 °C during winter and 25 and 28 °C in summer and 500 mm annual precipitation.

Table A1. Insulation data (U-values) for the building envelope (reinforced concrete structure).

Shell Type	Layers	U (W/m ² K)
Roof insulation	Reinforced concrete slab, extruded polystyrene, Lightweight concrete, ceramic tiles	0.272
Concrete column	Reinforced concrete, extruded polystyrene	0.324
Outside wall	Ceramic brick, extruded polystyrene, ceramic brick	0.319
Floor insulation	Reinforced concrete slab, extruded polystyrene	0.443

The insulation values that were used (Table A1) adhere to the stricter legislated standards in Greece. Double glazed windows are employed with $U = 1.29 \text{ W/m}^2\text{K}$ and $g = 0.333$ (Solar Heat Gain Coefficient). The window–wall ratio is 0.29 (average). Shading applied to the vertical openings, resulting to shading coefficients from 0.5 for the south-facing openings to 0.8 for the north-facing ones. Ventilation according to the requirements

of ASHRAE 62.2-2004 [45]. The operation schedule provides heating or cooling to the building during the working hours 8:00–20:00 on weekdays and 09:00–14:00 on Saturdays.

Table A2. Heating and cooling mode characteristics of the water–water heat pump.

Heating Mode	Ground Loop Water Temperature [°C]									
	18.0	15.0	13.0	10.0	8.5	7.0	4.5	2.0	0.0	
kW thermal	271.4	255.4	241.9	228.8	216.0	209.7	193.2	183.0	173.0	
KW	46.8	45.6	44.8	44	43.2	42.8	42	41.6	41.2	
COP	5.8	5.6	5.4	5.2	5	4.9	4.6	4.4	4.2	
Cooling Mode		Ground Loop Water Temperature [°C]								
		20	25	30	35	40	45			
kW thermal		201.6	198.9	196.1	194.2	185.6	177.8			
kW		48	51	53	55.5	58	63.5			
COP		4.2	3.9	3.7	3.5	3.2	2.8			

References

- GOV.UK. Pm to Announce Electric Vehicle Revolution. 2021. Available online: <https://www.gov.uk/government/news/pm-to-announce-electric-vehicle-revolution> (accessed on 20 July 2022).
- Funke, S.Á.; Sprei, F.; Gnann, T.; Plötz, P. How much charging infrastructure do electric vehicles need? A review of the evidence and international comparison. *Transp. Res. Part D Transp. Environ.* **2019**, *77*, 224–242. [CrossRef]
- Nicholas, M.; Lutsey, N. *Quantifying the Electric Vehicle Charging Infrastructure Gap in the United Kingdom*; ICCT: London, UK, 2020.
- Dreisbusch, M.; Mang, S.; Ried, S.; Kellerer, F.; Pfab, X. Regulation of Grid-efficient Charging from the User's Perspective. *MTZ Worldw.* **2020**, *81*, 66–70. [CrossRef]
- Engel, H.; Hensley, R.; Knupfer, S.; Sahdev, S. *The Potential Impact of Electric Vehicles on Global Energy Systems*; McKinsey Center for Future Mobility: Hong Kong, 2018.
- Fachrizal, R.; Shepero, M.; Aberg, M.; Munkhammar, J. Optimal PV-EV sizing at solar powered workplace charging stations with smart charging schemes considering self-consumption and self-sufficiency balance. *Appl. Energy* **2021**, *307*, 118139. [CrossRef]
- Osório, G.J.; Gough, M.; Lotfi, M.; Santos, S.F.; Espassandim, H.M.D.; Shafie-khah, M.; Catalao, J.P.S. Rooftop photovoltaic parking lots to support electric vehicles charging: A comprehensive survey. *Int. J. Electr. Power Energy Syst.* **2021**, *133*, 107274. [CrossRef]
- Bhatti, A.R.; Salam, Z.; Aziz, M.J.B.A.; Yee, K.P. A critical review of electric vehicle charging using solar photovoltaic. *Int. J. Energy Res.* **2016**, *40*, 439–461. [CrossRef]
- Casella, V.; Fernandez Valderrama, D.; Ferro, G.; Minciardi, R.; Paolucci, M.; Parodi, L.; Robba, M. Towards the Integration of Sustainable Transportation and Smart Grids: A Review on Electric Vehicles' Management. *Energies* **2022**, *15*, 4020. [CrossRef]
- Alkaws, G.; Baashar, Y.; Abbas, U.D.; Alkahtani, A.A.; Tiong, S.K. Review of Renewable Energy-Based Charging Infrastructure for Electric Vehicles. *Appl. Sci.* **2021**, *11*, 3847. [CrossRef]
- Love, J.; Smith, A.Z.P.; Watson, S.; Oikonomou, E.; Summerfield, A.; Gleeson, C.; Biddulph, P.; Chiu, L.F.; Wingfield, J.; Martin, C.; et al. The addition of heat pump electricity load profiles to GB electricity demand: Evidence from a heat pump field trial. *Appl. Energy* **2017**, *204*, 332–342. [CrossRef]
- Renault. The Energy Efficiency of an Electric Car Motor. 11 December 2021. Available online: <https://www.renaultgroup.com/en/news-on-air/news/the-energy-efficiency-of-an-electric-car-motor/> (accessed on 20 July 2022).
- Lebrouhi, B.E.; Schall, E.; Lamrani, B.; Chaibi, Y.; Kousksou, T. Energy Transition in France. *Sustainability* **2022**, *14*, 5818. [CrossRef]
- Bottarelli, M.; González Gallero, F.J. Energy Analysis of a Dual-Source Heat Pump Coupled with Phase Change Materials. *Energies* **2020**, *13*, 2933. [CrossRef]
- Angelopoulos, A.; Ktena, A.; Manasis, C.; Voliotis, S. Impact of a Periodic Power Source on a RES Microgrid. *Energies* **2019**, *12*, 1900. [CrossRef]
- Mele, E.D.; Elias, C.; Ktena, A. Machine Learning Platform for Profiling and Forecasting at Microgrid Level. *Electr. Control Commun. Eng.* **2019**, *15*, 21–29. [CrossRef]
- Roumpakias, E.; Stamatelos, T. Prediction of a Grid-Connected Photovoltaic Park's Output with Artificial Neural Networks Trained by Actual Performance Data. *Appl. Sci.* **2022**, *12*, 6458. [CrossRef]
- Schlachberger, D.P.; Brown, T.; Schramm, S.; Greiner, M. The benefits of cooperation in a highly renewable European electricity network. *Energy* **2017**, *134*, 469–481. [CrossRef]
- Cebulla, F.; Naegler, T.; Pohl, M. Electrical energy storage in highly renewable European energy systems: Capacity requirements, spatial distribution, and storage dispatch. *J. Energy Storage* **2017**, *14*, 211–223. [CrossRef]
- Protopapadaki, C.; Saelens, D. Heat pump and PV impact on residential low-voltage distribution grids as a function of building and district properties. *Appl. Energy* **2017**, *192*, 268–281. [CrossRef]

21. Bagalini, V.; Zhao, B.Y.; Wang, R.Z.; Desideri, U. Solar PV-Battery-Electric Grid-Based Energy System for Residential Applications: System Configuration and Viability. *Research* **2019**, *2019*, 3838603. [[CrossRef](#)]
22. Sørensen, Å.L.; Lindberg, K.B.; Sartori, I.; Andresen, I. Analysis of residential EV energy flexibility potential based on real-world charging reports and smart meter data. *Energy Build.* **2021**, *241*, 110923. [[CrossRef](#)]
23. Jufri, F.H.; Aryani, D.R.; Garniwa, I.; Sudiarto, B. Optimal Battery Energy Storage Dispatch Strategy for Small-Scale Isolated Hybrid Renewable Energy System with Different Load Profile Patterns. *Energies* **2021**, *14*, 3139. [[CrossRef](#)]
24. Zhen Huang, W.; Zaheeruddin, M.; Cho, S.H. Dynamic simulation of energy management control functions for HVAC systems in buildings. *Energy Convers. Manag.* **2006**, *47*, 926–943. [[CrossRef](#)]
25. AE. AE-A-Series EV Charger. Available online: <https://www.ae-electronics.com/> (accessed on 20 July 2022).
26. Zogou, O.; Stamatelos, A. Optimization of thermal performance of a building with ground source heat pump system. *Energy Convers. Manag.* **2007**, *48*, 2853–2863. [[CrossRef](#)]
27. Zogou, O.; Stamatelos, A. *Application of Building Energy Simulation in the Sizing and Design Optimization of an Office Building and Its HVAC Equipment*; Chapter 11 in *Energy and Buildings: Efficiency, Air Quality, and Conservation*; Utrick, J.B., Ed.; Nova Science Publishers: Hauppauge, NY, USA, 2009.
28. Thermal Energy System Specialists, LLC. *TRNSYS 16 Manual*; Solar Energy Laboratory, University of Wisconsin—Madison: Madison, WI, USA, 2005.
29. Safa, A.A.; Fung, A.S.; Kumar, R. Heating and cooling performance characterisation of ground source heat pump system by testing and TRNSYS simulation. *Renew. Energy* **2015**, *83*, 565–575. [[CrossRef](#)]
30. Neymark, J.; Judkoff, R.; Knabec, G.; Lec, H.-T.; Duerig, M.; Glasse, A.; Zweifele, G. Applying the building energy simulation test (BESTEST) diagnostic method to verification of space conditioning equipment models used in whole-building energy simulation programs. *Energy Build.* **2002**, *34*, 917–931. [[CrossRef](#)]
31. *ANSI/ASHRAE Standard 140–2001*; Standard Method of Test. for the Evaluation of Building Energy Analysis Computer Programs. ASHRAE: Atlanta, GA, USA, 2001.
32. Sharp. 375 Wp/Mono: NUJC375 Data Sheet. 2022. Available online: <https://www.sharp.eu/monocrystalline-solar-panels/375-wp-mono-nujc375> (accessed on 20 July 2022).
33. Thermal Energy System Specialists, LLC. *Component Libraries for TRNSYS, Version 2.0. User's Manual*; Solar Energy Laboratory, University of Wisconsin—Madison: Madison, WI, USA, 2004; Available online: <http://www.tess-inc.com/services/software> (accessed on 20 July 2022).
34. Saldaña, G.; San Martín, J.I.; Zamora, I.; Asensio, F.J.; Oñederra, O. Analysis of the Current Electric Battery Models for Electric Vehicle Simulation. *Energies* **2019**, *12*, 2750. [[CrossRef](#)]
35. Meng, J.; Luo, G.; Ricco, M.; Swierczynski, M.; Stroe, D.-I.; Teodorescu, R. Overview of Lithium-Ion Battery Modeling Methods for State-of-Charge Estimation in Electrical Vehicles. *Appl. Sci.* **2018**, *8*, 659. [[CrossRef](#)]
36. Hussein, A.A.; Batarseh, I. An overview of generic battery models. In *Proceedings of the 2011 IEEE Power and Energy Society General Meeting, Detroit, MI, USA, 24–28 July 2011*; pp. 1–6.
37. Sundén, B. Chapter 6—Thermal management of batteries. In *Hydrogen, Batteries and Fuel Cells*; Sundén, B., Ed.; Academic Press: Cambridge, MA, USA, 2019; pp. 93–110.
38. De Soto, W.; Klein, S.A.; Beckman, W.A. Improvement and validation of a model for photovoltaic array performance. *Solar Energy* **2006**, *80*, 78–88. [[CrossRef](#)]
39. Sang, J.; Liu, X.; Liang, C.; Feng, G.; Li, Z.; Wu, X.; Song, M. Differences between design expectations and actual operation of ground source heat pumps for green buildings in the cold region of northern China. *Energy* **2022**, *252*, 124077. [[CrossRef](#)]
40. Huang, S.; Zhu, K.; Dong, J.; Li, J.; Kong, W.; Jiang, Y.; Fang, Z. Heat transfer performance of deep borehole heat exchanger with different operation modes. *Renew. Energy* **2022**, *193*, 645–656. [[CrossRef](#)]
41. Wang, Y.; Wang, Y.; You, S.; Zheng, X.; Wei, S. Operation optimization of the coaxial deep borehole heat exchanger coupled with ground source heat pump for building heating. *Appl. Therm. Eng.* **2022**, *213*, 118656. [[CrossRef](#)]
42. Entsoe. Transparency Platform: Central Collection and Publication of Electricity Generation, Transportation and Consumption Data and Information for the Pan-European Market. 2022. Available online: <https://transparency.entsoe.eu/> (accessed on 20 July 2022).
43. Zappa, W.; Junginger, M.; van den Broek, M. Is a 100% renewable European power system feasible by 2050? *Appl. Energy* **2019**, *233–234*, 1027–1050. [[CrossRef](#)]
44. Zhang, Y.; Wik, T.; Bergström, J.; Pecht, M.; Zou, C. A machine learning-based framework for online prediction of battery ageing trajectory and lifetime using histogram data. *J. Power Sources* **2022**, *526*, 231110. [[CrossRef](#)]
45. *ANSI/ASHRAE Standard 62.2–2004*; Ventilation and Acceptable Indoor Air Quality in Low-Rise Residential Buildings. ASHRAE: Atlanta, GA, USA, 2004; p. 18.